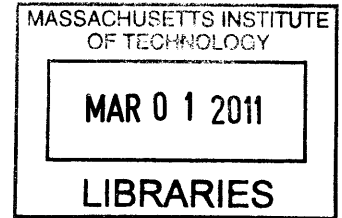


Investigation of Acquired Hearing Loss in  
Dopamine Beta Hydroxylase (DBH)-Mutant Mice

by

Suh-Kyung Lee

B.S., Mathematics and Psychology (2004)  
University of California, Los Angeles



SUBMITTED TO THE HARVARD-MIT DIVISION OF  
HEALTH SCIENCES AND TECHNOLOGY IN PARTIAL FULFILLMENT OF THE  
REQUIREMENTS FOR THE DEGREE OF

MASTER OF SCIENCE IN HEALTH SCIENCES AND TECHNOLOGY

AT THE

MASSACHUSETTS INSTITUTE OF TECHNOLOGY

**ARCHIVES**

FEBRUARY 2011

© 2011 Massachusetts Institute of Technology. All rights reserved.

Signature of Author .....  
Harvard-MIT Division of Health Sciences and Technology  
December 22, 2010

Certified by .....  
John J. Rosowski, PhD  
Professor of Otology & Laryngology and Health Sciences & Technology  
Thesis Supervisor

Accepted by .....  
Ram Sasisekharan, PhD  
Director, Harvard-MIT Division of Health Sciences and Technology  
Edward Hood Taplin Professor of Health Sciences & Technology and Biological Engineering



# Investigation of Acquired Hearing Loss in Dopamine Beta Hydroxylase (DBH)-Mutant Mice

by

Suh-Kyung Lee

Submitted to the Harvard-MIT Division of Health Sciences and Technology  
on December 22, 2010 in Partial Fulfillment of the  
Requirements for the Degree of Master of Science in  
Health Sciences and Technology

## ABSTRACT

The influence of middle-ear disease on hearing in mice is not well understood. We investigated middle-ear function and structure in a small group of dopamine beta hydroxylase (DBH)-knockout mice, which are known to be susceptible to middle-ear disease. We measured auditory brainstem response (ABR) and distortion-product otoacoustic emission (DPOAE) thresholds, as well as sound-induced umbo velocity, and used standard histological techniques to study normal and pathological middle-ear anatomy. Anatomical analyses included observation of tympanic membrane and ossicular structures, reconstruction of middle ear volume, and estimation of the volume of lightly or darkly stained middle-ear fluid. Lightly stained fluid in diseased ears was located throughout the middle ear, whereas darkly stained fluid, when present, was usually seen near the round window. The ABR and DPOAE thresholds and the umbo velocity produced by lower- and middle-frequency sound stimuli were strongly correlated with middle-ear air volume. The volume of darkly stained fluid was correlated with the DPOAE and ABR thresholds for lower- and middle-frequency sounds. The volume of lightly stained fluid was correlated with the umbo velocity in the middle and upper frequencies. Regression analyses between the thresholds and velocity show the DPOAE threshold about twice the ABR threshold in the middle frequencies, while the ABR threshold was roughly inversely proportional to the umbo velocity at lower stimulus frequencies. The correlations between histological and functional results are consistent with a decrease in middle-ear air volume and the presence of lightly stained fluid affecting the motion of the TM, while the darkly stained fluid near the round window acts to reduce the middle ear vibrations that reach the cochlea. The inverse relationship between the ABR threshold and the umbo velocity is consistent with a conductive hearing loss produced by reduced middle-ear air volume.

Thesis Supervisor: John J. Rosowski  
Title: Professor of Otology & Laryngology and Health Sciences & Technology  
Harvard Medical School, Boston, Massachusetts



**Contents**

Introduction ..... 7

Methods ..... 10

    1. *Animals*

    2. *Physiology*

    3. *Anatomy*

Results ..... 16

    1. *Umbo velocity transfer functions*

    2. *Qualitative analysis of the anatomy*

    3. *Estimation of fluid volume in the middle ear*

    4. *Regression analyses and correlations among the physiological measurements*

    5. *Correlations between anatomy and physiology*

    6. *Effect of DBH gene on middle ear anatomy and physiology*

    7. *Effect of potential measurement errors on the final analysis*

Discussion and Conclusion ..... 22

Acknowledgement ..... 24

References ..... 25

Tables and Figures ..... 26



## **Introduction**

Hearing loss can be categorized, depending on the site of pathology, as either conductive or sensorineural, where conductive hearing loss usually results from pathology within the external and/or middle ear(s) that interferes with the conduction of sound to the inner ear, and sensorineural hearing loss results from pathology within the inner ear and/or auditory regions of the brain that interferes with stimulation of the sensory cells or the neural transduction of sensory responses to or within the brain. Due to the differing degrees of 1) complexity in the nature of the dysfunction, 2) treatment involved, and perhaps most importantly, 3) prognosis for hearing improvement, characterizing the type of hearing loss is important for understanding how particular animal models of ear pathology relate to the human condition.

In this thesis, I report the results of investigations on middle-ear function and structure in a small group of dopamine  $\beta$ -hydroxylase (DBH)-knockout mice. DBH is an enzyme that converts dopamine to norepinephrine; thus deletion of the DBH gene causes an organism to lack norepinephrine, and in turn, to have a functionally impaired sympathetic nervous system. Researchers at Eaton-Peabody Laboratories, while studying auditory sensitivity in DBH-mutant mice to assess the role of adrenergic signaling in resistance to acoustic injury, discovered that there was a large variability in auditory brainstem response (ABR) and distortion-product otoacoustic emission (DPOAE) measurements of hearing sensitivity between different individuals of identical genetic background, and within the same individual as a function of time with repeated measurements (Maison et al. 2010). Since it was also determined that the DBH knockout mice were more susceptible to middle ear infections, a question was raised whether some of the hearing losses observed in these mice were conductive in nature and were secondary to the predilection in these animals for middle ear infections. Such a conclusion would greatly impact the investigation of whether any of the observed hearing loss was a direct result of a change in sympathetic innervation to the inner ear (Maison et al. 2010).

To investigate whether the variability of hearing sensitivity in these animals had its root in different degrees of middle ear disease within the population, I began a study of middle-ear function and structure in a collection of these mice with a wide range of auditory thresholds. The population of mice I tested is described in Table 1 and included three heterozygous DBH knockouts (+/-) and one homozygous wild type (+/+).

Figure 1 shows the variability in the two different measures of hearing function (ABR and DPOAE) made on the two ears of these four mice. The figure illustrates a wide variability in the hearing responses of the six ears of three heterozygous mice, compared to the two ears of the homozygous wild type. The right ear of (+/-) mouse 398 and the left ear of (+/-) mouse 8279 show hearing sensitivity that is generally better (lower ABR and DPOAE thresholds) than that of the two ears of the (+/+) mouse 8280, while the other four heterozygous ears show hearing thresholds that are significantly higher than the homozygous ears, particularly at the low and middle frequencies. It should also be noted that the DPOAE threshold increases are larger than the increases observed in the ABR thresholds. As discussed in the next paragraph, this is an indication of a conductive hearing pathology.

The contribution of middle-ear sound conduction to ABR and DPOAE can be described as follows: The sound energy from the stimulus flows through the external ear to reach the tympanic membrane, which gives rise to ossicular motions in the middle ear cavity. This mechanical energy is transduced in the inner ear, where specialized sensory cells generate (i) synaptic release that activates the neural pathway and produces the ABR, and (ii) electro-mechanical signals that send sound energy back to the external ear via the middle ear in the form of DPOAEs. Since DPOAEs depend on sound energy traveling forwards through the middle ear to the inner ear to initiate the sensory processes, and then the return journey of the inner-ear-generated distortions backwards through the middle ear to the external ear, sound energy travels through the middle ear twice in DPOAE generation and measurement, as opposed to once in ABR. Therefore, any middle ear pathology is expected to have a greater effect on DPOAE than on ABR (Qin et al. 2010). Moreover, the middle ear is generally considered to be a linear system, and thus changes in middle-ear sound conduction would be reflected as a simple change in the gain of the sound transfer function through the middle ear (Qin et al. 2010). A series of experiments carried out by Qin et al. (2010) demonstrated that an artificial conductive pathology generally produced a change in DPOAE thresholds (in dB) that are 1.5-2.5 times larger than ABR threshold change (in dB) at frequencies less than 30 kHz.

In order to investigate the possibility that some of the variability in hearing seen in the DBH-mutant population was the results of varying degrees of conductive hearing loss induced by middle ear disease, I directly measured middle-ear function in these animals using laser-Doppler vibrometry to ascertain the sound-induced motion of the tympanic membrane (Rosowski et al.



2003). I also performed an anatomical investigation of the condition of the middle ears in the different animals to determine the presence of ear pathology and quantify alterations in middle-ear structure, especially the presence of fluid in the middle ear. Finally, I correlated the physiological measurements of hearing threshold and middle-ear function with my anatomical findings.

## Methods

### *1. Animals*

Four adult female mice of hybrid strain 129/SvCPJ x C57BL/6 were used in this study. Heterozygous knockouts for DBH were obtained from Steven Thomas of the University of Pennsylvania. The deletion of the DBH gene and the breeding of the hetero- and homozygous mutants have been described (Thomas et al. 1995, 1998). The four mice used in this study were born on March 13, 2007. Three mice were heterozygous for DBH knockout and one was a wild type. The genetic makeup of the mice is summarized in Table 1. All procedures were reviewed and approved by the Animal Care Committee of the Massachusetts Eye and Ear Infirmary.

### *2. Physiology*

#### *2.1 ABR and DPOAE measurements*

Mice were anesthetized (pentobarbital, 71.2 mg/kg IP), and measurements of ABR and DPOAE were made in a soundproof chamber with the temperature maintained near 32 °C. A small cut was made in the cartilaginous ear canal to allow microscopic examination of the tympanic membrane and to better couple the sound delivery system to the ear. Tone-burst stimuli were generated digitally (National Instruments, digital I-O board 6052E), and were delivered using a custom acoustic assembly consisting of two Tucker Davis electrostatic earphones to deliver primary tones and a Knowles miniature microphone to record ear-canal sound pressure. Ear-canal pressure and electrode voltage responses were amplified and digitally sampled at 20  $\mu$ s for analysis (Maison et al. 2010).

For ABR measurements, needle electrodes were inserted at the vertex and the pinna, while the ground electrode was placed near the tail. The stimuli of 5-ms tone pips (0.5-ms rise-fall with a  $\cos^2$  onset) were delivered at 35 /s, and the response was amplified ( $10^4$ x), filtered (0.1-3 kHz), digitized, and averaged in a LabVIEW-based data-acquisition system. The frequency of the tone pips varied between 0.5 kHz and 50 kHz at roughly half-octave intervals. At each frequency, the sound level was varied from low to high, but never exceeded 80 dB SPL. At each stimulus level, 1024 responses were averaged with alternating stimulus polarity. Stimulus level was increased in 5-dB steps up to 80 dB SPL from 10 dB below the threshold, where “threshold” was defined as the lowest SPL in which any response waveform could be detected

visually; this level usually corresponded to the level step just below that at which peak-to-peak response amplitude rose significantly above the noise floor (Maison et al. 2010).

For DPOAE measurements at  $2f_1-f_2$ , the primary-tone ratio ( $f_2/f_1$ ) was 1.2, and  $f_2$  level was 10 dB below  $f_1$  level. Each pair of primary tone levels was swept in 5-dB steps from 20 dB SPL to 80 dB SPL (for  $f_2$ ). At each stimulus level, waveform and spectral averaging was used to increase the signal-to-noise ratio of the ear-canal sound pressure, and the amplitude of DPOAE ( $2f_1-f_2$ ) was extracted from the averaged spectra. “Threshold” was defined as the  $f_1$  level required to produce a DPOAE at 0 dB SPL (Maison et al. 2010).

All eight ears were tested for ABR and DPOAE. Mice were allowed to recover from surgery after these measurements, and laser-Doppler measurements of umbo velocity were made one to two weeks later.

## *2.2 Umbo velocity measurements*

The umbo is the tip of the malleus handle embedded within the tympanic membrane near the center of the roughly circular membrane. Mice were anesthetized (ketamine, 100 mg/kg IP; xylazine, 10 mg/kg IP), with booster injections of 1/3-1/2 the original dose as needed. Body temperature was maintained near 37 °C by a heating pad within a heated sound chamber (Qin et al. 2010). The pinna was removed and a small section of the bony external-ear canal removed to visualize the umbo.

A Polytec laser-Doppler vibrometer (LDV) was used to measure sound-induced umbo velocity in six of the eight ears (398L, 8279L, 8280R/L, 8282R/L). The experimental procedure of measuring the motions of the umbo within the tympanic membrane closely follows that of Rosowski et al. (2003). A small piece of autoreflective tape containing three to four 50- $\mu$ m-diameter balls was placed on the lateral surface of the tympanic membrane that was coupled to the manubrium close to the umbo. A cylindrical brass coupler with a side-arm sound entry port was used to steady the head of the mouse and to control the sound field at the entrance of the ear canal. The laser was focused on the reflective beads over the umbo through the open back of the brass coupler (Figure 2).

The sound stimuli consisted of broad-band chirps containing frequencies between 1 kHz and 50 kHz that were generated by a DOS-based desktop computer with a DSP16+ signal processing board using SYSid. The generated stimulus signal was amplified by a power amplifier and then

delivered to a Beyerdynamic DT-48 earphone that generated the acoustic signal presented to the ear. The resulting sound signals varied between 80 dB SPL and 100 dB SPL in level. The laser beam was focused on the umbo reflectors through the brass coupler and the LDV response was measured by SYSid. After the LDV measurement, a probe-tube microphone was placed into the entrance of the ear canal for a separate measurement of sound pressure using the identical sound stimulus. (Noise floor was also measured with the absence of sound stimulus, so that an optimal frequency range for the LDV and the microphone measurements could be determined. Frequencies below 1 kHz gave a small signal-to-noise ratio for the umbo velocity measurement, and frequencies above 21 kHz for the sound pressure measurement.) An independent calibration of the probe-tube microphone was done to convert the microphone's voltage response into sound pressure. The *umbo velocity transfer function* was then computed from the ratio of the complex amplitudes of the umbo velocity and the sound pressure at each stimulus frequency.

Data filtered at every third of an octave were used for analysis, and thus stimulus frequency values that matched those of ABR and DPOAE measurements were approximate: 5.6 kHz data were collected from 5.01 kHz, 8 kHz data from 7.94 kHz, 11.3 kHz data from 10 kHz, 16 kHz data from 15.8 kHz, 22.6 kHz data from 25.1 kHz, 32 kHz data from 31.6 kHz, and 45.2 kHz data from 50.1 kHz.

Umbo velocity transfer functions were only measured in six ears (Figure 3) as two ears were damaged during the surgical preparation and placement of reflective beads.

### 3. *Anatomy*

#### 3.1 *Histological preparation*

After the measurement of sound-induced umbo velocity in the anesthetized mice, the mice were euthanized with an overdose of ketamine and xylazine. The mice were then decapitated and the heads placed in fixative (of 2.5% glutaraldehyde and 1.5% paraformaldehyde) for 5 to 20 days. The fixed heads were decalcified in EDTA, osmicated, dehydrated in ethanol and propylene oxide, osmicated, embedded in araldite, and sectioned on a HistoRange at 20 microns. The majority of the embedded heads were sectioned so that the mid-modiolar view of the inner ear would be visible in the same plane as a section through the round window and the crura of the stapes with sections removed from ventral to dorsal (Maison et al. 2010). In such a scheme, the

sections are roughly perpendicular to the stapes footplate and the round window is sectioned before the oval window. In ears 398L and 8280L, the plane of sectioning was such that the resulting sections were roughly parallel to the footplate and perpendicular to the crura of the stapes. Seven of the eight ears (398R/L, 8279R/L, 8280R/L, and 8282L) were prepared in total, and each ear produced 110-140 sections. Sections were mounted and coverslipped.

### *3.2 Qualitative data analysis*

Images of mouse temporal bone sections were taken using a compound microscope with a 2x objective coupled to a color camera. ImageJ (NIH) was used for qualitative analysis of middle-ear anatomy and for calibration (scale: 0.272 pixels/ $\mu\text{m}$ ). In the sections, I looked for presence of stained material within the middle-ear air spaces (suggesting the presence of middle-ear fluid), the connections between and orientation of the ossicles (malleus, incus, and stapes), condition of the middle-ear muscles (tensor tympani and stapedius), and the presence of perforations in the tympanic membrane.

### *3.3 Quantitative data acquisition and analysis*

#### *3.3.1 Initial estimation of middle ear volume*

Amira software was used for 3D reconstruction of the mouse middle-ear structures from the histological sections. To reduce the memory load on the computer performing the reconstructions, every other or every third image was stacked and aligned using a semi-automatic procedure. Thus, the thickness of each layer in the reconstructions is either 40  $\mu\text{m}$  (when every other section was used in the reconstruction) or 60  $\mu\text{m}$  (when every third was used). Initial observations suggested the presence of significant amounts of light and dark staining material within the middle-ear spaces that are normally filled with air, which we interpreted as the presence of middle ear effusions. One challenge with the osmium staining was how to separate out the different effusions from the bone. I decided on color ranges that could classify each pixel of the middle-ear images into four subcategories: air, bone (including malleus, incus, and stapes), light fluid, and dark fluid, according to structural boundaries or shades. The normal middle-ear cavity is defined by the boundaries of the bulla, with a lateral boundary at the tympanic membrane, and the medial boundary at the medial wall of the skull and the edge of tensor tympani muscle.

A coin-stacked 3D reconstruction of the middle ear was generated from the sequence of categorized areas, and the volume of each structure was computed. The total volume of the bounded middle-ear cavity was then computed by summing the four volumes:

$$\text{Total} = \text{Air} + \text{Ossicles} + \text{Light fluid} + \text{Dark fluid}.$$

The stapedia artery was excluded from the total volume. In the severely diseased ear 398L, a thick membrane surrounding the ossicles was not included in the total volume; on the other hand, tensor tympani and other fragmented structures within the middle ear were included in the air volume.

### *3.3.2 New estimation of middle ear volume*

Histological sections of some ears (398R and 8279L) were missing the dorsal and/or ventral boundaries of the normal middle-ear cavity. Thus, the actual (Air, Ossicle, and Total) volumes must be larger than the estimate. The volume of missing middle-ear structures for 398R and 8279L was estimated from cross-sectional areas of a reference ear 8282L using ImageJ. 8282L was selected due to its similar cutting plane as 398R and 8279L, and finer thickness (40  $\mu\text{m}$  as opposed to 60  $\mu\text{m}$ ) used for reconstruction and volume measurement. (8282L had moderate abnormality including small middle-ear space, but nonetheless suggested a larger volume error than using 8280L with 60- $\mu\text{m}$  thickness as a reference.) The dorsal and/or ventral volume segment of the reference ear starting from the image with middle-ear space comparable to that of the last available image in 398R and 8279L was estimated and added to the volumes of the two ears. As a result of such compensation, the volume of 398R was increased by less than 5% of the Total and the volume of 8279L was increased by less than 8% of the Total.

The bulla of 8280R appears to have been detached from the petrous bone during the embedding stage, and the middle ear structures in the sections are greatly damaged. Looking at the progression of structural changes along the image sequence, I used my best judgment to fully locate tympanic membrane boundaries and to eliminate potentially artifactual “air” space. Two independent measurements of the total volume made using Amira and ImageJ differed by 1%. I used the mean value of the two estimates in the final result.

For some ears, the Eustachian tube opening is included in the air space. However, this volume is small relative to the Total. Considering the proportion of missing volume in 398R, this error (toward having a larger total volume) is expected to be smaller than 5% of the Total.

### 3.3.3 “Dark” fluid vs. “Light” fluid

Defining fluid as either dark or light was based on both gray value and apparent consistency of material. Due to variations in transmitted light within the microscope and camera, there was an inherent variation in light intensity from the anterior to posterior side of the digitized images.

My original *Light* fluid volume estimates of 8280R and 8280L were significantly confounded by this gradient. Although light intensity was not identical across ear images, gray values of the assigned subcategories generally satisfy  $50 < \textit{Dark fluid} < 110 < \textit{Light fluid} < 160 < \textit{Air} < 210$ .

*Dark* fluid also has a thicker, more solid-like appearance than *Light* fluid. For subsequent, more conservative estimation made with ImageJ, boundary conditions for gray values were  $|\textit{Air} - \textit{Light fluid}| \approx 40$  or less, while  $|\textit{Air} - \textit{Dark fluid}| > 50$ .

## Results

### *1. Umbo velocity transfer functions*

The frequency and the magnitude of the umbo velocity transfer function from six individual ears are shown in Figure 3. The umbo velocity (in units of mm/s) normalized by the sound pressure of the sound stimulus in the ear canal (in units of pascals) was converted to an inverse dB scale of  $20 \cdot \log_{10}(\text{velocity}/\text{sound pressure})$  with 1 (mm/s)/Pa as the reference value. The mean umbo velocity and the standard deviation of 20 control CBA/CaJ mice from Qin et al. (2010) are used as a comparison. With an exception of 8279L at low frequencies, all of the measured ears show decreased umbo movement (plotted on the inverted dB ordinate scale) at nearly all frequencies compared to the control CBA/CaJ ears. There was also significant variability within the measured velocity from this study's ears. The largest variations are observable at frequencies of 10 kHz and below. Ear 398L displays a low magnitude of umbo velocity (high inverted dB value) throughout the measured frequency range. Some of the differences between the mice in this study and the CBA/CaJs of Qin et al. (2010) may be related to differences in middle-ear function between different strains of mice (Rosowski et al. 2003).

### *2. Qualitative analysis of the anatomy*

The histological preparation method used in these ears yielded several artifact problems and was not optimal for studying the middle ear anatomy. For example, some of the middle ear structures, especially the more fragile tympanic membrane, manubrium, and the thin bulla wall appear to have been damaged during the sectioning process. Without regard to the condition of the tympanic membrane, I was able to characterize the middle ear anatomy of four to six (out of seven) ears reliably.

Images of two sectioned ears from the homozygous control mouse 8280 are shown in Figure 4. For each ear, sections are presented from ventral to dorsal: near the round window opening (left column), near the oval window and the appearance of the malleus (middle), and after the appearance of the incudo-malleal joint and the pars flaccida of TM (right). The left ear (upper panel) of 8280 has few apparent structural abnormalities other than damaged TM around the manubrium and slightly darker posterior region of the middle-ear air space (a2 and a3), which may be due to the choice of staining or the light intensity during image capture. In addition to middle ear pathology, the right ear of mouse 8280 (b1, b2, and b3) is more affected by sectioning



artifact than the left ear: The bulla appears to have been dislocated from the petrous bone during preparation, and possibly as a result, the lateral portion of the middle-ear structure including the pars flaccida of TM is missing. Furthermore, the fractured manubrium and the dislocated stapes footplate and incudo-malleal and incudo-stapedial joints may be at least partially explained by faulty sectioning. However, there is also evidence of middle-ear fluid near the Eustachian tube opening and around the incus (b3), as suggested by darker staining in these areas.

Ears from the heterozygous mice showed a large variability in their middle ear anatomy. Figure 5 shows sections of three heterozygous ears that demonstrate large differences including normal appearance (upper panel), moderate abnormality (middle panel), and severe abnormality (lower panel) of the middle ear. The left ear of mouse 8279 (8279L) has a healthy middle ear with clear middle-ear air space and intact TM, ossicles, and middle-ear muscles. 8282L shows a moderate amount of middle-ear abnormality, where darkly stained material suggesting chronic middle-ear effusion is visible in the round window niche (b1), and the TM and the malleus are medialized so that the manubrium comes into contact with the lateral part of the tensor tympani muscle (b2). The ventral portion of the orbicular apophysis of malleus appears to be in close contact with the medial wall of the middle ear space (not shown). The incudo-malleal joint is also up against the medial wall - more prominently than other ears (e.g., 398R in Figure 6a); pars flaccida is torn posteriorly (b3).

The left ear of 398 exhibits the most severely abnormal middle-ear anatomy among the seven specimens examined in this thesis. Darkly and lightly stained material is visible near the round window (c1), and lightly stained material in the middle-ear air space behind the TM (c2). The tensor tympani is also significantly damaged such that the ventral portion is torn into two pieces (c2). At a more dorsal section (c3), the malleus appears to be fractured at the lamina and the orbicular apophysis is rotated laterally by 90 degrees along the axis of the manubrium. Furthermore, the incudo-malleal joint surrounded by a thickened membrane is pushing up against the medial wall of the temporal bone. The portion of these abnormalities due to sectioning artifact is not known, though the presence of dark and light fluid near the round window is likely not an artifact.

The remaining heterozygous ears are shown in Figure 6. 398R shows mild abnormality with lightly stained material in the posterior-dorsal part of the middle ear space (a3). Damaged pars tensa and fractured malleus are also visible (a2) but could be artifacts. 8279R exhibits a greater

degree of middle ear pathology with stained materials near the round window (b1), the Eustachian tube (b2 and b3), and the oval window (b3). The manubrium and the TM appear to be damaged and sucked in medially.

### *3. Estimation of fluid volume in the middle ear*

Simple dark/light contrast makes it difficult to determine the source of alterations in gray, i.e., whether from anomalies (e.g., effusion, thickened membrane), from the normal structures (e.g., muscles, nerve fibers), or from artifacts (e.g., gradient in light intensity during image acquisition, especially in 8280R/L, exterior fluid and a crease - the embedding material appears to have been slightly folded before being placed on the slide and so gives differing gray values in adjacent regions - in 8280L). In addition, the presence of Light fluid and its boundaries within the middle ear cavity are not clear in some images, e.g., 398R, 8280R/L. For these reasons, I made an alternative “more conservative” estimate of fluid volumes in six ears using ImageJ based on gray values as described in the methods. Total volume was also reevaluated for two ears that showed severe natural and/or artifactual disruption in the middle ear space: 398L and 8280R.

Table 2 reports the mean value of the two separate estimations of fluid volume, except for Light fluid in 8280R and 8280L and Dark fluid in 8280R, for which the new conservative estimates were judged to be more accurate. For Total volume, the original estimates from Amira are used aside from the four ears: 398R, 398L, 8279L, and 8280R. Air volume computation was done by subtracting the other measured volumes from the Total volume:

$$\text{Air} = \text{Total} - \text{Dark fluid} - \text{Light fluid} - \text{Ossicles}$$

In other words, Air volume was assigned to be most variable and dependent particularly on the new estimate of fluid volumes.

### *4. Regression analyses and correlations among the physiological measurements*

Linear least-squares regression analyses were performed between pairs of the three physiological measurements: ABR and DPOAE, ABR and umbo velocity (dB), and DPOAE and umbo velocity (dB), and including t-tests on the regression coefficient. For DPOAE vs. ABR, t-tests investigating whether the dB value of the change in DPOAE thresholds was twice the dB change of ABR thresholds were performed to test the doubling effect of middle-ear disease on DPOAE relative to ABR that is predicted by simple models of conductive hearing loss (Qin et al. 2010).

Significant regression fits between the changes in ABR and DPOAE thresholds were observed at mid frequencies, with a slope of near 2 at 16 kHz and 22.6 kHz and with a slope of near 1 at 11.3 kHz (Table 3). Zero correlation at the lowest and the highest frequencies were due to thresholds reaching the maximum stimulus sound level set at 80 dB SPL for ABR and 85 dB SPL for DPOAE. Regressions between the ABR thresholds and the dB magnitude of the umbo velocity transfer function were performed, along with t-tests comparing the regression slopes to -1 since a negative correlation between TM mobility and ABR threshold is expected with middle ear disease, especially when middle-ear effusion is present (Qin et al. 2010). Correlations between ABR and umbo velocity were significant at low frequencies; the slope was found to be statistically indistinguishable from -1 at 5.6 kHz, 8 kHz, and 11.3 kHz (Table 4). DPOAE and umbo velocity data were not strongly correlated at most frequencies; significant negative correlations were found only between umbo velocity (dB) at 5.6 kHz and DPOAE at mid frequencies (11.3 kHz, 16 kHz, and 22.6 kHz), and between umbo velocity (dB) at 8 kHz and DPOAE at 16 kHz.

##### *5. Correlations between anatomy and physiology*

Variations in middle-ear “cleanliness”, demonstrated in the anatomical measurements (ME total volume and fluid volume) with respect to the physiological measurements (ABR, DPOAE, and umbo velocity), were analyzed. As shown in Table 5, ABR thresholds were negatively correlated with Total volume ( $\mu\text{L}$ ) at low and mid frequencies ( $p < 0.01$  at 5.6 kHz, 8 kHz, 11.3 kHz, and 16 kHz;  $p < 0.05$  at 22.6 kHz); positively correlated with Dark fluid volume (%) at low and mid frequencies ( $p < 0.005$  at 5.6 kHz, 8 kHz, and 11.3 kHz;  $p < 0.05$  at 16 kHz and 22.6 kHz), but with Dark fluid volume ( $\mu\text{L}$ ) only at low frequencies ( $p < 0.05$  at 5.6 kHz, 8 kHz, and 11.3 kHz). DPOAE thresholds were also negatively correlated with Total volume ( $\mu\text{L}$ ) at mid frequencies ( $p < 0.01$  at 11.3 kHz, 16 kHz, and 22.6 kHz); positively correlated with Dark fluid volume at mid frequencies (in %,  $p < 0.005$  and in  $\mu\text{L}$ ,  $p < 0.05$  at 11.3 kHz, 16 kHz, and 22.6 kHz). Umbo velocities (dB) were positively correlated with Total volume at low frequencies ( $p < 0.005$  at 5.6 kHz and 8 kHz;  $p < 0.05$  at 11.3 kHz); negatively correlated with Light fluid volume at mid frequencies (in %,  $p < 0.01$  at 16 kHz and  $p < 0.05$  at 22.6 kHz; in  $\mu\text{L}$ ,  $p < 0.05$  at 16 kHz, 22.6 kHz, and 32 kHz). Figure 7 plots linear regression of Total volume ( $\mu\text{L}$ ) and fluid

volume (%) against physiological data at two mid frequencies (11.3 kHz and 16 kHz, respectively), with the intercepts and slopes indicated in Table 5.

Table 5 further demonstrates that the amount of correlation with physiological data is dependent on whether ME fluid is measured in the absolute volume ( $\mu\text{L}$ ) or in percentage of a given ME total volume. Total volume variation is largely dependent on Air volume variation, since the proportion of air is much greater than that of fluid or ossicles. Dark & Light fluid volume is largely dependent on Light fluid volume, since the proportion of Light fluid usually outweighs that of Dark fluid when both fluids are present.

When analyzed for correlations among the anatomical data, strong negative correlation between Dark fluid volume (%) and Total volume ( $\mu\text{L}$ ) was observed.

#### *6. Effect of DBH gene on middle ear anatomy and physiology*

With all mice controlled for age, I tested whether variations in all measurements - DPOAE, ABR, umbo velocity, ME total volume, and ME fluid volume (both in  $\mu\text{L}$  and in %) - were similar across genotype. Two-sample t-test assuming unequal variance on genotype (heterozygous vs. wildtype) was performed. Sample size was small ( $N = 4$  to  $6$  for heterozygous, HZ;  $N = 2$  for wildtype, WT). No group difference in umbo velocity, total volume, and fluid volume was found. DPOAE data showed that at 22.6 kHz, HZ has higher thresholds than WT; at 45.7 kHz, WT has higher thresholds than HZ. (However, at 45.7 kHz, DPOAE reached the maximum SPL for both of the WT ears and thus the variance is zero.) ABR results showed that at 5.6 kHz and 22.6 kHz, HZ has higher thresholds than WT.

#### *7. Effect of potential measurement errors on the final analysis*

To see the effect of volume measurement errors on the final analysis, I obtained correlations results using alternative volume data.

##### *7.1 Conservative fluid volume estimates*

New conservative values of Light fluid volume for 398R, 8279R, 8280R, and 8280L; Dark fluid volume for 398L, 8279R, 8280R, and 8282L; and Total volume for 398L replaced the corresponding values reported in Table 2. Total (Air) volume vs. physiology data (ABR, DPOAE, and umbo velocity) shows the same frequency dependence in significant correlations as

in the previous analysis (with different p-values). Dark fluid volume (%) is correlated with ABR at identical frequencies except for 22.6 kHz and with umbo velocity at 5.6 kHz ( $p < 0.05$ ). Dark fluid volume ( $\mu\text{L}$ ) is correlated with DPOAE only at 16 kHz ( $p < 0.05$ ), while Dark fluid volume (%) is correlated with DPOAE at identical frequencies as shown in Table 5. Light fluid volume ( $\mu\text{L}$  and %) and Dark & Light volume ( $\mu\text{L}$  and %) are also correlated with umbo velocity at identical frequencies ( $p < 0.05$ ).

### 7.2 *Simple mean of all estimates*

For each fluid-filled ear, I averaged all estimates of Light fluid volume and Dark fluid volume, respectively. I also used the mean value of Total volume estimates for 398L. Total (Air) volume vs. ABR, DPOAE, and umbo velocity shows the same frequency dependence in significant correlations as in Table 5. Correlations between Dark fluid volume ( $\mu\text{L}$  and %) and physiology data also demonstrate the same frequency dependence. Light fluid volume ( $\mu\text{L}$ ) is correlated with umbo velocity only at 22.6 kHz, and Light fluid volume (%) at 22.6 kHz and 32 kHz ( $p < 0.05$ ). Dark & Light fluid volume shows correlations with umbo velocity at higher frequencies than suggested in the previous analysis (in  $\mu\text{L}$ , at 22.6 kHz and 45.7 kHz; in %, at 22.6 kHz, 32 kHz, and 45.7 kHz).

### 7.3 *Dark fluid near the round window*

I also analyzed the data by only including Dark fluid volume near the round window for 398L, 8279R, and 8280R. (Dark fluid volume estimate for 8282L was not altered since all dark stains were present near the round window.) Light fluid volume data used were identical to those presented in Table 2. Total (Air) volume vs. ABR, DPOAE, and umbo velocity shows the same frequency dependence in significant correlations as in Table 5. Dark fluid volume ( $\mu\text{L}$ ) is correlated with ABR at 5.6 kHz and 8 kHz, and with DPOAE only at 22.6 kHz ( $p < 0.05$ ). Dark fluid volume (%) is less strongly correlated with ABR ( $p < 0.05$  at 5.6 kHz, 8 kHz, and 16 kHz) and DPOAE ( $p < 0.05$  at 16 kHz and 22.6 kHz) than suggested in Table 5. Light fluid volume ( $\mu\text{L}$  and %) and Dark & Light fluid volume ( $\mu\text{L}$  and %) are correlated with umbo velocity at identical frequencies as shown in Table 5.

## Discussion and Conclusion

The results shown in Table 5 and Figure 7 demonstrate that the ears with a small middle-ear total volume and a large fraction of dark fluid volume had increased ABR and DPOAE thresholds at mid frequencies (11.3 kHz, 16 kHz, and 22.6 kHz). 398L and 8279R had the smallest middle-ear total volume as well as the largest fractions of middle-ear (dark) fluid volume (Table 2). Their ABR and DPOAE thresholds were two of the worst among eight ears in overall frequencies (Figure 1). 8282L with the next highest overall hearing thresholds had correspondingly small total volume and large fraction of dark fluid volume but not light fluid volume (Table 2, Figure 1), suggesting that the amount of dark fluid near the round window has a greater effect on hearing thresholds than the amount of light fluid present throughout the middle ear space.

Looking at the TM motions, the ears with an elevated ABR threshold were associated with a decreased umbo velocity at low frequencies (5.6 kHz, 8 kHz, and 11.3 kHz), demonstrating the inverse relationship between the ABR threshold and the umbo velocity in cases of a conductive hearing loss (Table 4). Although DPOAE and umbo velocity data from six ears were not strongly correlated, the ears with the worst DPOAE thresholds - 398L, 8282L, and 8282R - were shown to have the worst umbo velocities at low frequencies (Figures 1 and 3). Having a large fraction of light fluid volume was also associated with a decreased umbo velocity at mid frequencies (Table 5).

These histological and functional findings are consistent with the idea that a reduced middle-ear air volume - due to either a small middle-ear cavity or the presence of light fluid - affects the motion of the TM, and the presence of dark fluid near the round window acts to reduce the middle ear vibrations that reach the cochlea. This claim is further supported by the larger change in DPOAE thresholds compared to ABR thresholds by a factor of near 2 at 16 kHz and 22.6 kHz (Table 3). In summary, it is likely that changes in middle ear produced by the onset of middle-ear disease are responsible for changes in hearing thresholds in these mice.

For future experiments, the choice of histological preparation could be improved for greater durability to minimize damage in the middle ear structures, and for greater specificity to enhance structural boundaries within the middle ear space. A larger sample size would clarify the effects of middle ear anatomy on hearing thresholds, and with a balanced number of homozygous knockout (-/-), heterozygous knockout (+/-), and wildtype (+/+) ears and with a

variation of age, would demonstrate susceptibility of middle ear pathology in DBH-mutant mice. Furthermore, setting a higher maximum stimulus sound levels for ABR and DPOAE measurements may allow us to determine correlations at all stimulus frequencies.

## **Acknowledgement**

I thank Melissa Wood, Haobing Wang, and Erik Larsen for their assistance in data collection and for helpful comments. Work supported by NIDCD.



## References

- Maison, S.F., Le, M., Larsen, E., Lee, S.-K., Rosowski, J.J., Thomas, S.A., Liberman, M.C. (2010). Mice lacking adrenergic signaling have normal cochlear responses and normal resistance to acoustic injury but enhanced susceptibility to middle ear infection. *J. Assoc. Res. Otolaryngol.* 11, 449-61.
- Qin, Z., Wood, M., Rosowski, J.J. (2010). Measurement of conductive hearing loss in mice. *Hear. Res.* 263, 93–103.
- Rosowski, J.J., Brinsko, K.M., Tempel, B.L., Kujawa, S.G. (2003). The aging of the middle ear in 129S6/SvEvTac and CBA/CAJ mice. Measurements of umbo velocity, hearing function and the incidence of pathology. *J. Assoc. Res. Otolaryngol.* 4, 371–383.
- Saunders, J.C., Summers, R.M. (1982). Auditory structure and function in the mouse middle ear: an evaluation by SEM and capacitive probe. *J. Comp. Physiol. A* 146, 517–525.
- Thomas, S.A., Matsumoto, A.M., Palmiter, R.D. (1995). Noradrenaline is essential for mouse fetal development. *Nature* 374, 643–646.
- Thomas, S.A., Marck, B.T., Palmiter, R.D., Matsumoto, A.M. (1998). Restoration of norepinephrine and reversal of phenotypes in mice lacking dopamine beta-hydroxylase. *J. Neurochem.* 70, 2468–2476.

## Tables and Figures

Table 1. Mouse genotypes for dopamine beta-hydroxylase.

Mouse	398	8279	8280	8282
Genotype	+/-	+/-	+/+	+/-

Table 2. (a) Categorized ME volumes in the seven ears.

Volume (mm <sup>3</sup> or μL)	398R	398L	8279R	8279L	8280R	8280L*	8282L
Air	3.548	1.524	1.778	4.474	3.344	3.584*	2.437
Ossicles	0.1334	0.1394	0.1216	0.1481	0.1402	0.1478	0.1440
<i>Dark fluid</i>	0	0.0233	0.0223	0	0.0218	0	0.0283
<i>Light fluid</i>	0.1228	0.3338	0.1314	0	0.0688	0*	0
D&L fluid	0.1228	0.3571	0.1537	0	0.0906	0*	0.0283
Total	3.804	2.020	2.054	4.622	3.575	3.732	2.610

\*Presence of Light fluid is inconclusive due to light intensity, slide conditions, etc.

(b) Proportions of fluid in the total ME space.

% of Total Volume	398R	398L	8279R	8279L	8280R	8280L*	8282L
% Dark	0	1.15	1.09	0	0.609	0	1.08
% Light	3.23	16.5	6.40	0	1.92	0*	0
% D&L	3.23	17.7	7.48	0	2.53	0*	1.08

Table 3. One-sample *t*-test results on the slope of significantly correlated DPOAE and ABR pairs at a given frequency (with  $df = 7$ ; a  $|t| \leq 2.365$  points to a lack of difference between the measured slope and the target).

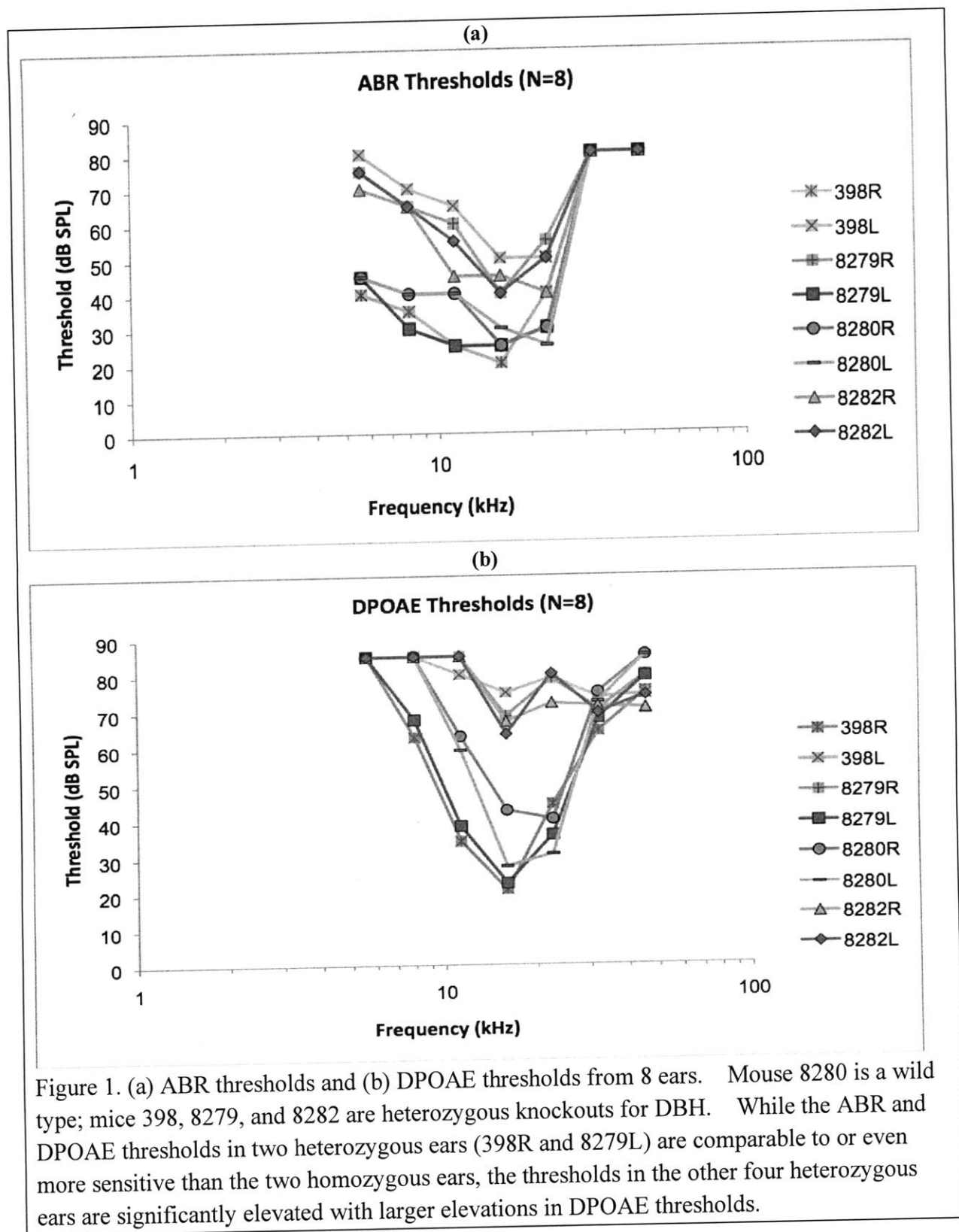
Frequency (Hz)	Slope	<i>Standard Error</i>	<i>p</i> -Value	<i>t</i> -Score, Slope = 1	<i>t</i> -Score, Slope = 2
5600	0	0	n/a		
8000	0.385	0.167	0.06		
11300	1.27	0.0248	0.00219*	<b>1.089</b>	
16000	1.94	0.315	0.000837*	2.984	<b>-0.19</b>
22600	1.82	0.302	0.000928*	2.715	<b>-0.596</b>
32000	0	0	n/a		
45700	0	0	n/a		

Table 4. One-sample *t*-test results on the slope of significantly correlated umbo velocity (dB) and ABR pairs at a given frequency ( $df = 5$ ,  $|t| \leq 2.571$ ).

Frequency (Hz)	Slope	<i>Standard Error</i>	<i>p</i> -Value	<i>t</i> -Score, Slope = -1
5600	-0.75	0.145	0.00662*	<b>1.724</b>
8000	-0.788	0.26	0.0386*	<b>0.808</b>
11300	-1.05	0.219	0.00885*	<b>-0.228</b>
16000	-0.646	0.474	0.245	
22600	0.165	0.471	0.744	
32000	0	0	n/a	
45700	0	0	n/a	

Table 5. Significant correlations between ME total volume and threshold (N = 7) or umbo velocity (N = 5) measurements, and between ME fluid volume and threshold (N = 7) or umbo velocity (N = 5) measurements.

Dependent Variable	Independent Variable	p-Value	Intercept	Slope
Total Volume ( $\mu\text{L}$ )	ABR_5600 (dB SPL)	0.00364	6.15571	-0.05105
	ABR_8000	0.00026	6.03906	-0.05756
	ABR_11300	0.00078	5.78766	-0.05838
	ABR_16000	0.00915	5.85954	-0.08087
	ABR_22600	0.01266	6.06550	-0.07158
	DP_11300 Hz (dB SPL)	0.00653	5.85514	-0.04172
	DP_16000	0.00106	5.07093	-0.04077
	DP_22600	0.00388	5.43077	-0.04012
	Vel_5600 (dB)	0.00121	4.81056	0.06695
	Vel_8000	0.00148	4.31446	0.05674
	Vel_11300	0.02051	4.11818	0.05485
	Air Volume ( $\mu\text{L}$ )	1.5095E-06	0.48853	0.91818
	% Dark Fluid	ABR_5600	0.00249	-1.11746
ABR_8000		0.00150	-0.98224	0.03133
ABR_11300		0.00259	-0.84710	0.03182
ABR_16000		0.01478	-0.88491	0.04404
ABR_22600		0.02312	-0.97220	0.03835
DP_11300		0.00308	-0.97361	0.02415
DP_16000		0.00004	-0.52722	0.02377
DP_22600		0.00289	-0.70227	0.02276
Vel_5600		0.03113	-0.19250	-0.03402
Vel_8000		0.02433	0.05132	-0.02930
% Light Fluid	Vel_16000	0.00980	-4.85939	-0.53098
	Vel_22600	0.04234	-4.80526	-0.55587
% Dark & Light Fluid	Vel_11300	0.03945	-1.51854	-0.39290
	Vel_16000	0.01254	-4.63699	-0.55252
Dark Fluid Volume ( $\mu\text{L}$ )	ABR_5600	0.03092	-0.02008	0.00058
	ABR_8000	0.02102	-0.01806	0.00064
	ABR_11300	0.02096	-0.01574	0.00066
	DP_11300	0.00840	-0.02065	0.00054
	DP_16000	0.00517	-0.00965	0.00051
	DP_22600	0.02681	-0.01222	0.00047
Light Fluid Volume ( $\mu\text{L}$ )	Vel_16000	0.02096	-0.08592	-0.01034
	Vel_22600	0.02897	-0.09435	-0.01144
	Vel_32000	0.03973	-0.27097	-0.01475
Dark & Light Fluid Volume ( $\mu\text{L}$ )	Vel_11300	0.04838	-0.01806	-0.00770
	Vel_16000	0.02922	-0.07539	-0.01059
	Vel_22600	0.04064	-0.08305	-0.01166
	Light Fluid Volume ( $\mu\text{L}$ )	2.9138E-06	0.01017	1.03730



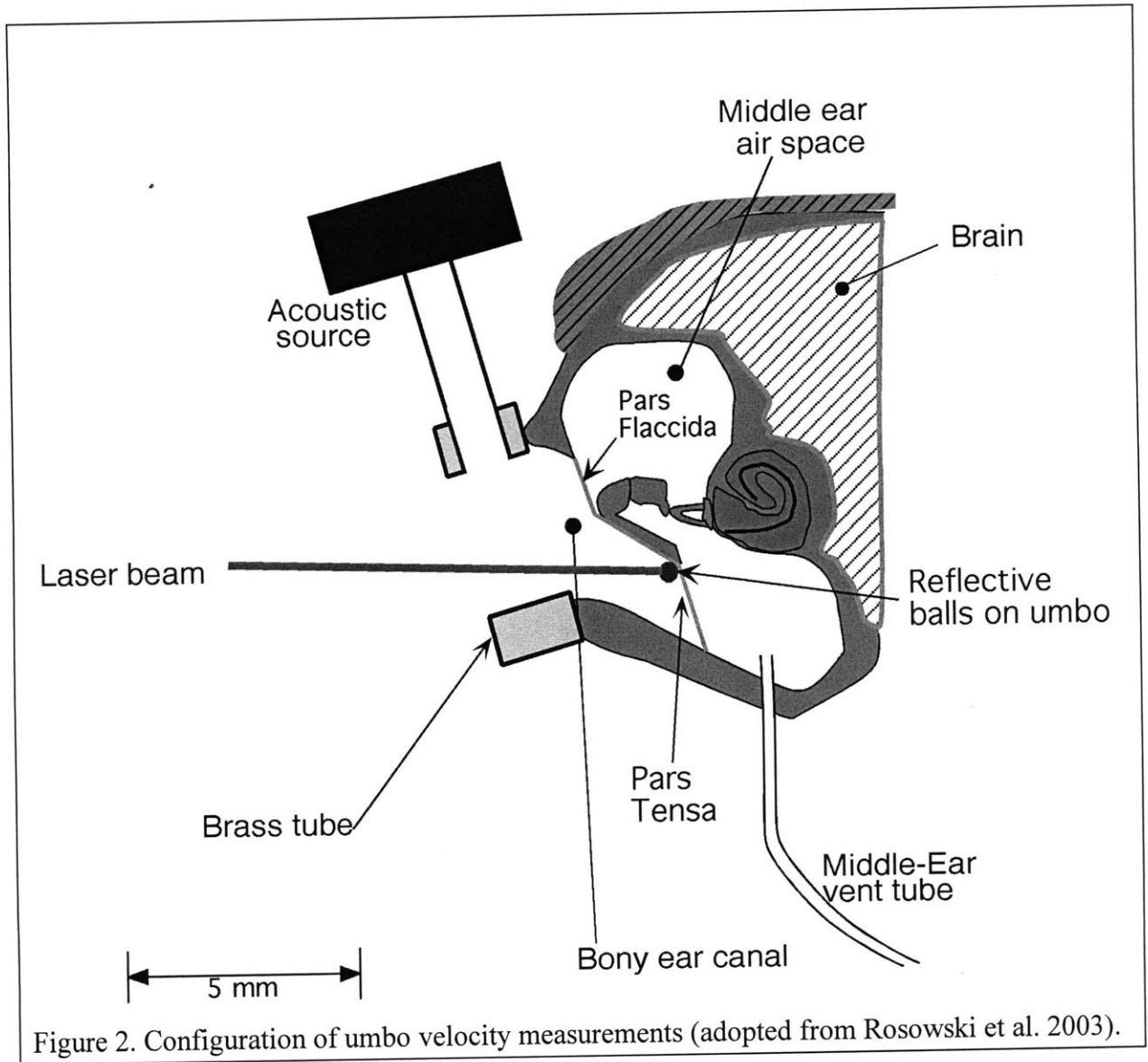
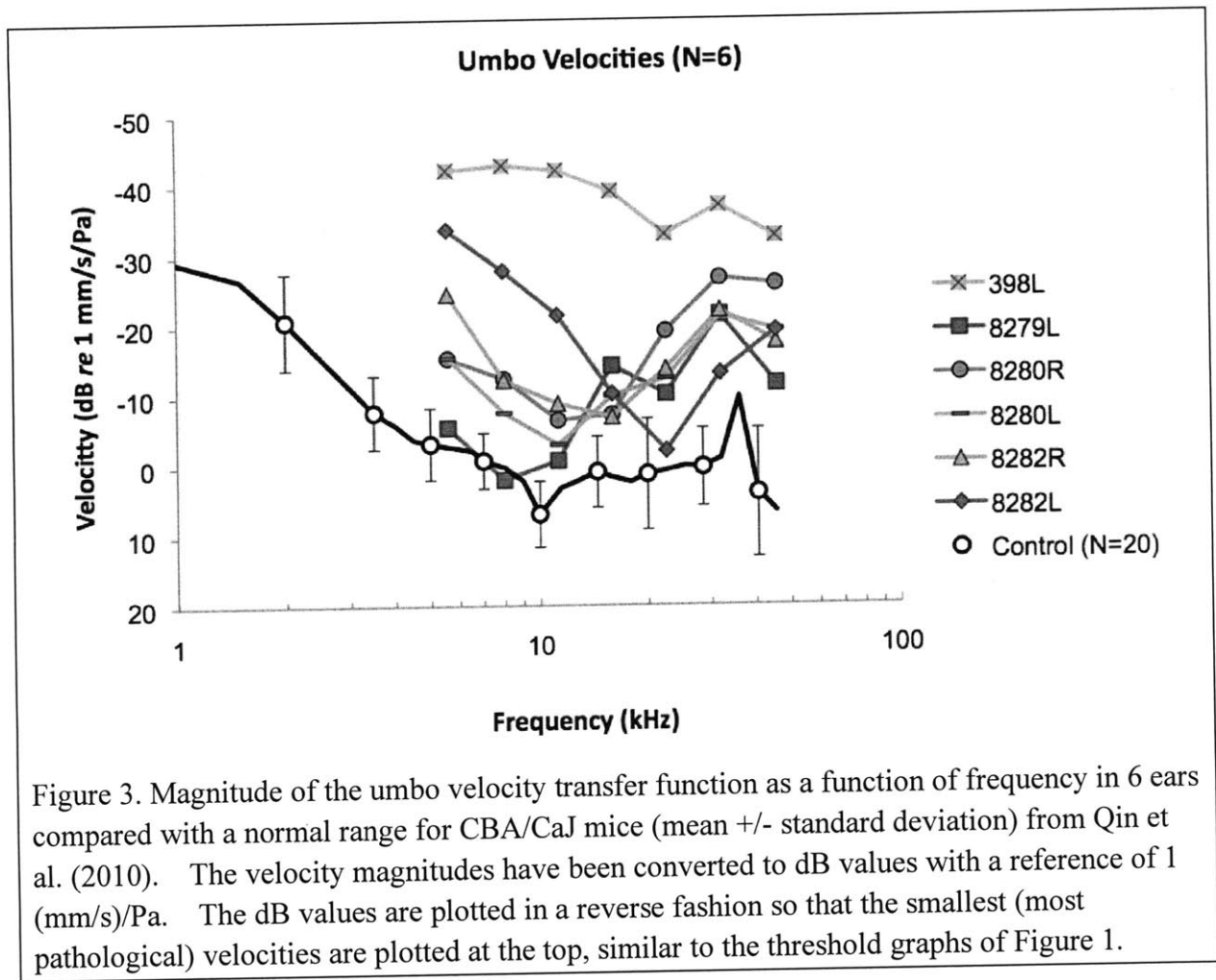


Figure 2. Configuration of umbo velocity measurements (adopted from Rosowski et al. 2003).





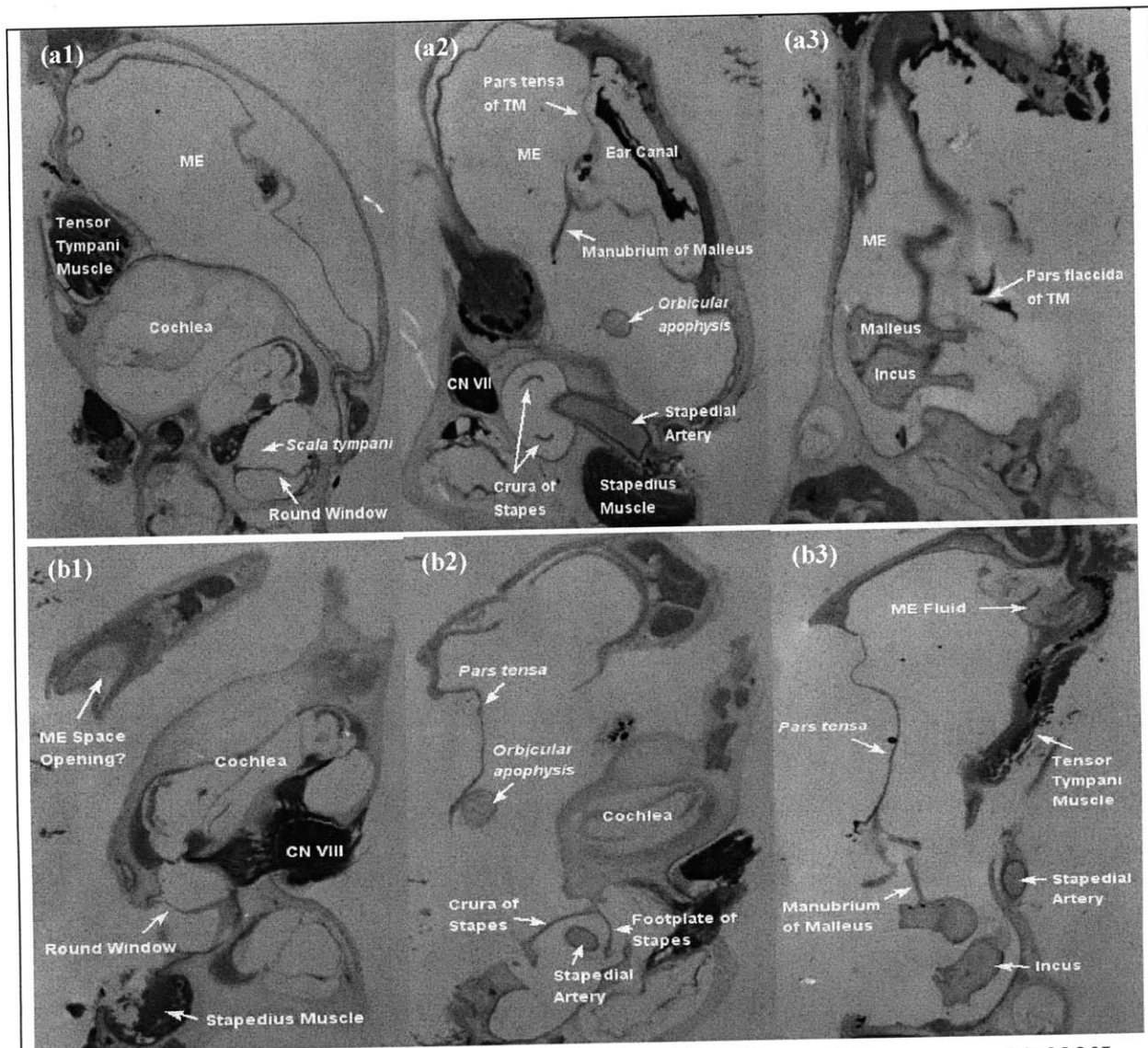


Figure 4. Three sections illustrating the middle ear anatomy from wildtype ears. (a) 8280L and (b) 8280R. The middle ear cavity is labeled ME, the tympanic membrane TM, and the cranial nerve CN. The *pars tensa* and *pars flaccida* are parts of the TM. The orbicular apophysis is part of the malleus (Saunders and Summers 1982). The stapedial artery travels through the middle ear cavity of the mouse and passes through the crura of the stapes.

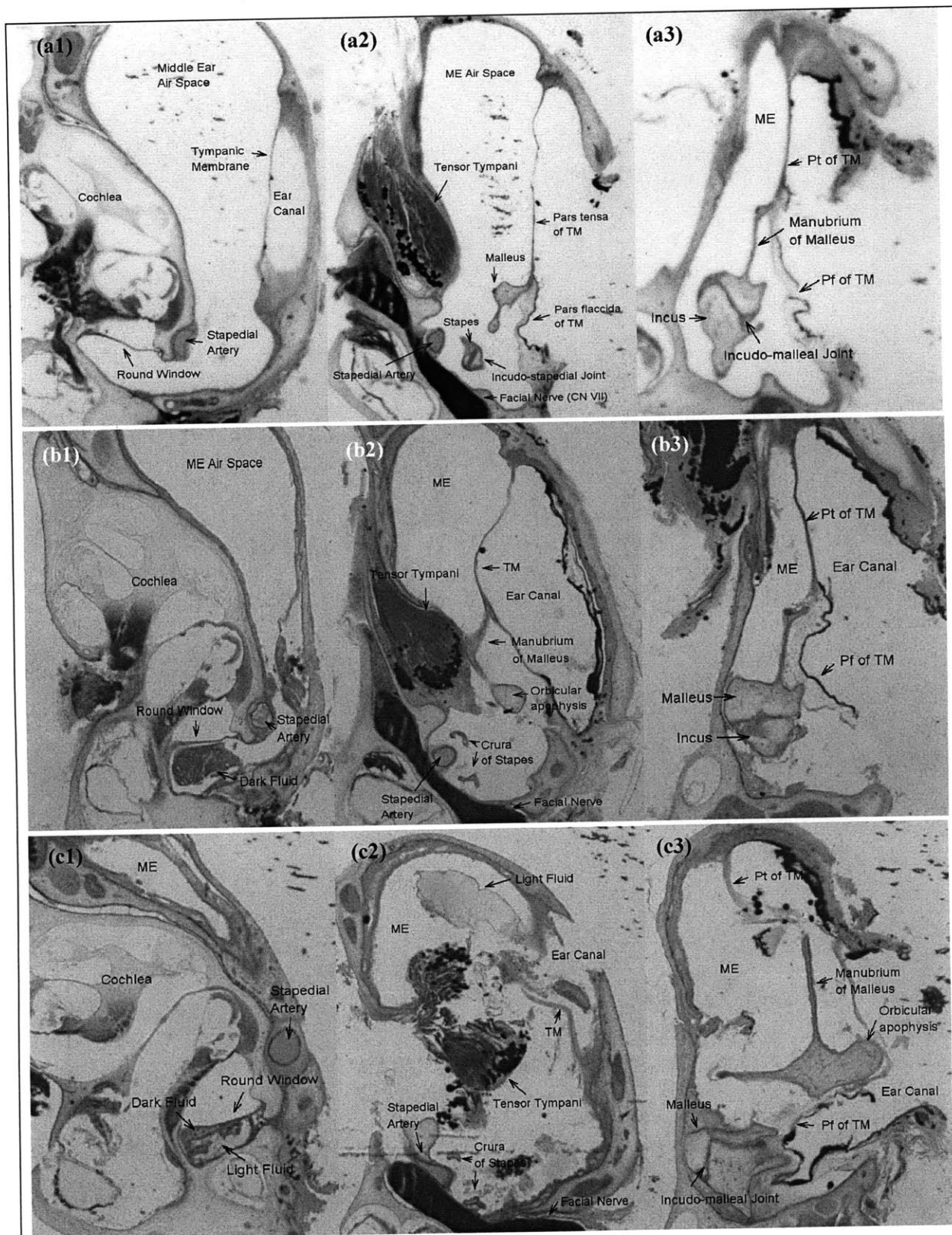


Figure 5. Middle ear anatomy from DBH heterozygous knockouts. (a) 8279L “normal” ear; (b) 8282L with moderate abnormality; (c) 398L with severe abnormality.

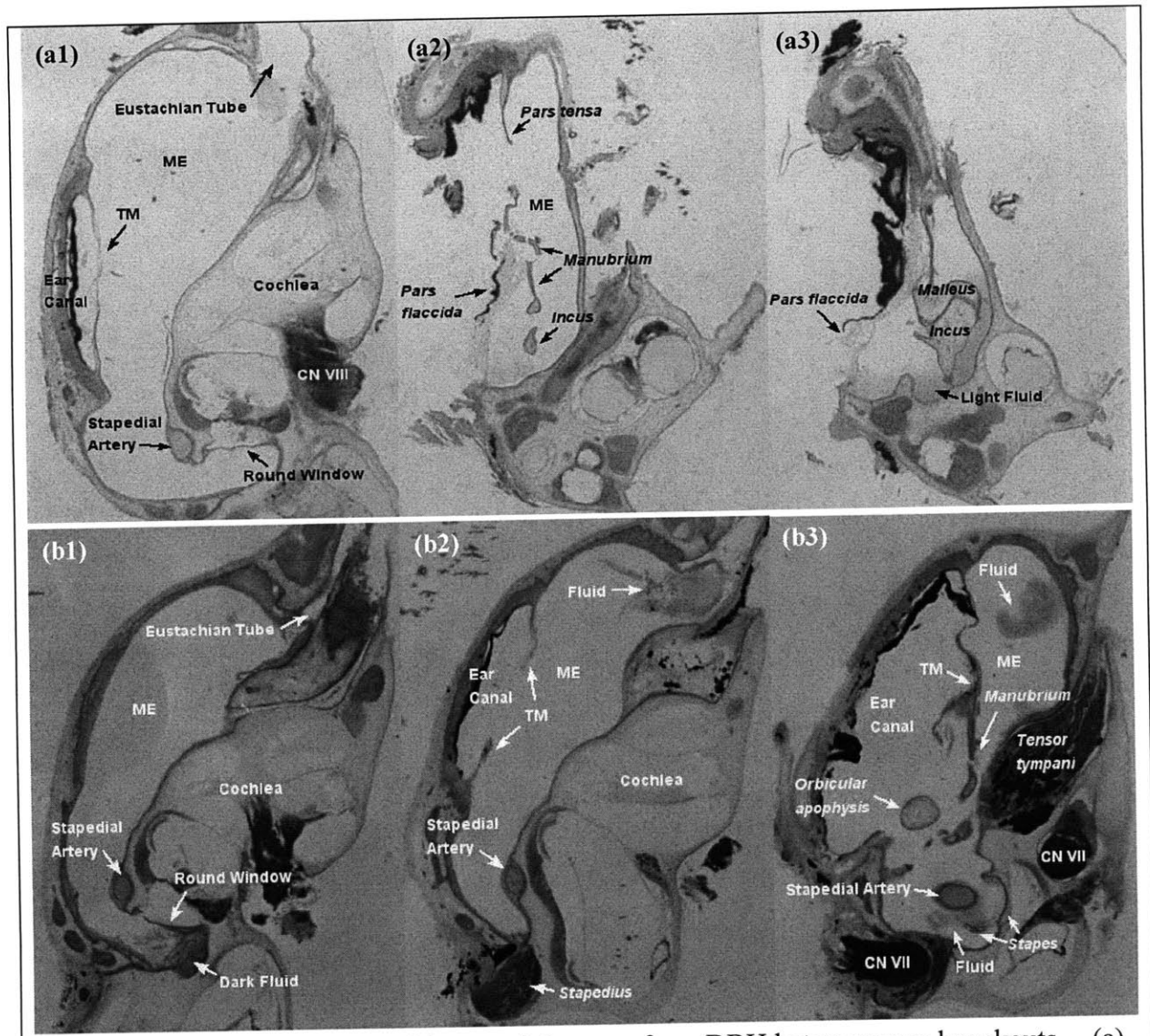


Figure 6. Middle ear anatomy of the remaining ears from DBH heterozygous knockouts. (a) 398R with mild abnormality; (b) 8279R with moderate abnormality.

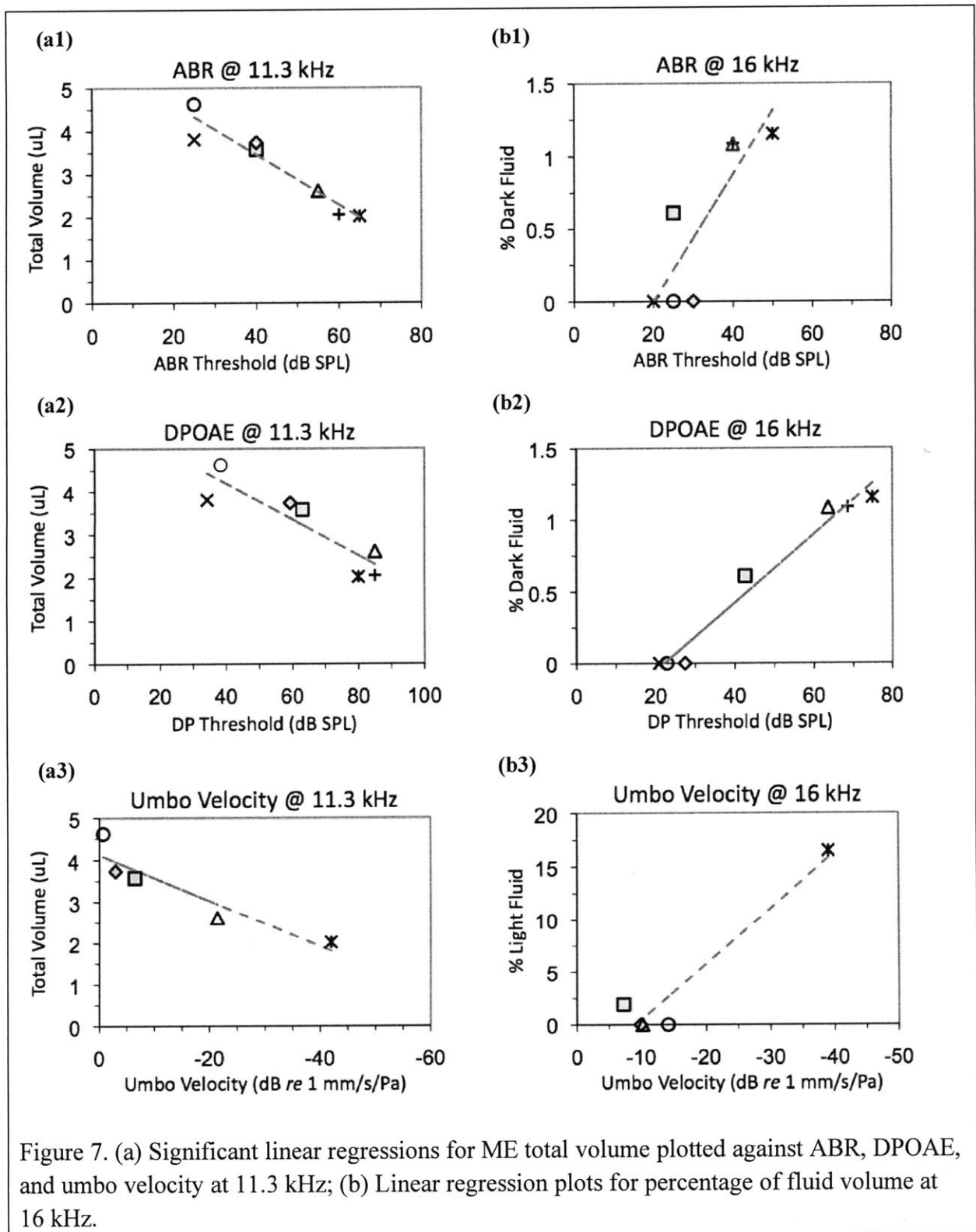


Figure 7. (a) Significant linear regressions for ME total volume plotted against ABR, DPOAE, and umbo velocity at 11.3 kHz; (b) Linear regression plots for percentage of fluid volume at 16 kHz.